REPORT DOCUMENTATION PAGE

Form Approved
OMB No. 0704-0188

PLEASE DO NOT RETURN YOUR FORM TO THE ABOVE ORGANIZATION.

1. REPORT DATE *(DD-MM-YYYY)*	2. REPORT TYPE	3. DATES COVERED *(From - To)*
07-11-2007	Journal Article	

4. TITLE AND SUBTITLE

Estimating The Underwater Light Field from Remote Sensing of Ocean Color

5a. CONTRACT NUMBER

5b. GRANT NUMBER

5c. PROGRAM ELEMENT NUMBER

0602435N

6. AUTHOR(S)

Cheng-Chien Liu, Richard L. Miller, Kendall L. Carder, Zhongping Lee, Eurico J. D'Sa, James E. Ivey

5d. PROJECT NUMBER

5e. TASK NUMBER

5f. WORK UNIT NUMBER

73-6802-06-5

7. PERFORMING ORGANIZATION NAME(S) AND ADDRESS(ES)

Naval Research Laboratory
Oceanography Division
Stennis Space Center, MS 39529-5004

8. PERFORMING ORGANIZATION REPORT NUMBER

NRL/JA/7330-06-6145

9. SPONSORING/MONITORING AGENCY NAME(S) AND ADDRESS(ES)

Office of Naval Research
800 N. Quincy St.
Arlington, VA 22217-5660

10. SPONSOR/MONITOR'S ACRONYM(S)

ONR

11. SPONSOR/MONITOR'S REPORT NUMBER(S)

12. DISTRIBUTION/AVAILABILITY STATEMENT

Approved for public release, distribution is unlimited.

13. SUPPLEMENTARY NOTES

14. ABSTRACT

We present a new approach that incorporates two models to estimate the underwater light field from remote sensing of ocean color. The first employs a series of analytical, semi-analytical, and empirical algorithms to retrieve the spectrum of inherent optical properties (IOPs), including the absorption and backscatter coefficients, from the spectrum of remote sensing reflectance. The second model computes the profile of photosynthetically available radiation E0,PAR(z) for a vertically homogeneous water column using the information of the retrieved IOPs and the ambient optical environment. This computation is based on an improved look-up table technology that posesses high accuracy, comparable with the full solution of the radiative transfer equations, and meets the computational requirement of remote sensing application. This new approach was validated by in situ measurements and an extensive model-to-model comparison with a wide range of IOPs. We successfully mapped the compensation depth by applying this new approach to process the SeaWiFS imagery. This research suggests that E0,PAR(z) can be obtained routinely from ocean-color data and may have significant implications for the estimation of global heat and carbon budget.

15. SUBJECT TERMS

photosynthetically available radiation, ocean color, radiative transfer, ocean optics, compensation depth

16. SECURITY CLASSIFICATION OF:			17. LIMITATION OF ABSTRACT	18. NUMBER OF PAGES	19a. NAME OF RESPONSIBLE PERSON
a. REPORT	b. ABSTRACT	c. THIS PAGE			Zhongping Lee
Unclassified	Unclassified	Unclassified	UL	14	19b. TELEPHONE NUMBER *(Include area code)* 228-688-4873

Journal of Oceanography, Vol. 62, pp. 235 to 248, 2006

Estimating the Underwater Light Field from Remote Sensing of Ocean Color

CHENG-CHIEN LIU[1]*, RICHARD L. MILLER[2], KENDALL L. CARDER[3], ZHONGPING LEE[4], EURICO J. D'SA[5] and JAMES E. IVEY[3]

[1]*Department of Earth Sciences, National Cheng Kung University, Tainan, Taiwan 701, R.O.C. also at Disaster Prevention Research Center and Earth Dynamic System Research Center, National Cheng Kung University, Tainan, Taiwan 701, R.O.C.*
[2]*NASA, Earth Science Applications Directorate, Stennis Space Center, MS 39529, U.S.A.*
[3]*College of Marine Science, University of South Florida, St. Petersburg, FL 33701, U.S.A.*
[4]*Naval Research Laboratory, Code 7340, Stennis Space Center, MS 39529, U.S.A.*
[5]*Department of Oceanography and Coastal Sciences, Louisiana State University, Baton Rouge, LA 70803, U.S.A.*

(Received 15 September 2005; in revised form 12 December 2005; accepted 12 December 2005)

We present a new approach that incorporates two models to estimate the underwater light field from remote sensing of ocean color. The first employs a series of analytical, semi-analytical, and empirical algorithms to retrieve the spectrum of inherent optical properties (IOPs), including the absorption and the backscatter coefficients, from the spectrum of remote sensing reflectance. The second model computes the profile of photosynthetically available radiation $E_{0,PAR}(z)$ for a vertically homogeneous water column using the information of the retrieved IOPs and the ambient optical environment. This computation is based on an improved look-up table technology that possesses high accuracy, comparable with the full solution of the radiative transfer equation, and meets the computational requirement of remote sensing application. This new approach was validated by *in situ* measurements and an extensive model-to-model comparison with a wide range of IOPs. We successfully mapped the compensation depth by applying this new approach to process the SeaWiFS imagery. This research suggests that $E_{0,PAR}(z)$ can be obtained routinely from ocean-color data and may have significant implications for the estimation of global heat and carbon budget.

Keywords:
· Photosynthetically available radiation,
· ocean color,
· radiative transfer,
· ocean optics,
· compensation depth.

1. Introduction

Observing ocean color from space is an important international tool in resource management and scientific investigations. Currently, there are ten space-borne ocean-color sensors orbiting the Earth operated by various space agencies in the United States, Asia and Europe. Another six satellites with ocean-color sensors onboard are scheduled to be launched in the next four years (http://www.ioccg.org/sensors_ioccg.html). A major goal of these missions is to assess the role that the ocean plays in the global carbon cycle and to examine the factors that affect global climate change (Hooker *et al.*, 1992). To attain this goal, the amount, distribution and productivity of phytoplankton must be estimated from space. Many past efforts have focused on relating radiative signals to pigment concentration (Gordon *et al.*, 1988; O'Reilly *et al.*, 1998; Carder *et al.*, 1999). Maps of satellite-derived pigment concentration (e.g., biomass) have been widely used to estimate global ocean carbon content and productivity (Longhurst, 1995; Platt *et al.*, 1995). However, rates of phytoplankton photosynthesis are regulated by many factors, including light availability. Hence, an accurate estimation of ocean primary production and carbon flux requires a thorough description of the underwater light field.

Compared to advanced methods for retrieving pigment concentrations from ocean color (Gordon *et al.*, 1988; O'Reilly *et al.*, 1998; Carder *et al.*, 1999), methods for estimating the underwater light field from space have not progressed very far. A common approach is to diminish the surface solar irradiance based on satellite-derived estimates of the diffuse attenuation coefficient for the downwelling planar irradiance K_{Ed} (symbols used in this paper are summarized in appendices) at 490 nm.

* Corresponding author. E-mail: ccliu88@mail.ncku.edu.tw

Table 1. Various values of the coefficients used in Eq. (1) taken from various past works.

$K_{Ed,water}(490)$	A	B	λ_1	λ_2	Source
0.022	0.088	−1.491	443	550	(Austin and Petzold, 1981)
0.022	0.0984	−1.403	443	550	(Mueller, 1995)
0.022	0.1	−1.3	443	555	(Mueller and Trees, 1997)
0.016	0.15645	−1.5401	490	555	(Mueller, 2000)

Based on a simple linear regression analysis on the data set, Austin and Petzold (1981) proposed the first empirical algorithm of $K_{Ed}(490)$ of the form:

$$K_{Ed}(490) = K_{Ed,water}(490) + A\left[\frac{L_w(\lambda_1)}{L_w(\lambda_2)}\right]^B, \qquad (1)$$

where $K_{Ed,water}(490)$ is the diffuse attenuation coefficient for pure water at wavelength 490 nm, $L_w(\lambda_1)$ and $L_w(\lambda_2)$ are water-leaving radiances at the respective wavelengths of λ_1 and λ_2. After new profiles were added to the data set, the values of the coefficients used in Eq. (1) had to be revised to maintain a better model-to-data fit. Table 1 lists various results of regression analysis from a series of works performed in the past.

There are four major known sources of error, however, involved in using this $K_{Ed}(490)$-based approach. First, K_{Ed} should be spectrally dependent. Measurements of K_{Ed} at one spectral band (e.g. 490 nm) cannot represent the spectrally dependent absorption of short- and long-wave components of light, even in the upper 10 m of the ocean (Simpson and Dickey, 1981). Second, K_{Ed} should be a function of depth even in a homogeneous medium (Zaneveld, 1989). Taking an average value of K_{Ed} over the first optical depth to propagate the light field throughout the water column may generate large errors at greater depths. Third, light absorption by phytoplankton or other water constituents generally have no preferential direction (Kirk, 1994). Current K_{Ed} models only calculate the downwelling planar irradiance E_d, yet should include the scalar irradiance E_0 for heat and carbon budgets. Fourth, the underwater light field is closely related to the sky radiance (diffuse) distribution at the sea surface, which is very sensitive to solar position (Liu *et al.*, 2002). A value of K_{Ed} obtained during a satellite overpass provides no information on the underwater light field at other times during the day.

Over the past two decades, major advances in radiative transfer theory have enabled a realistic numerical simulation of the underwater light field (Mobley *et al.*, 1993), provided that the inherent optical properties (IOPs) and the ambient optical environment are given. These radiative transfer models, however, have not attempted to conduct global simulations at the spatial resolution of ocean-color sensors, mainly due to the significant computational effort required to solve the full radiative transfer equation.

We present a new approach that incorporates two models to estimate the underwater light field from remote sensing of ocean color. The first employs a series of analytical, semi-analytical and empirical algorithms to retrieve the spectrum of inherent optical properties (IOPs), including the absorption and the backscatter coefficients, from the spectrum of remote sensing reflectance (Lee *et al.*, 2002). The second model computes the profile of photosynthetically available radiation $E_{0,PAR}(z)$ for a vertically homogeneous water column based on the information of the retrieved IOPs and the ambient optical environment (Liu *et al.*, 2002). This computation is based on an improved look-up table (LUT) technology that possesses a high accuracy, comparable with the full solution of the radiative transfer equation and meets the computational requirement of remote sensing application.

This new approach was first validated against *in situ* measurements. To further examine the applicability of this new approach for a large variety of water types, an extensive model-to-model comparison was then performed for a wide range of IOP combinations. The results show that the K_{Ed} approach generates substantial errors under different computational conditions, while our model reduces the errors significantly. This new approach was also applied to the SeaWiFS imagery to generate a map of the compensation depth. The premise assumptions of the set of three-variable bio-optical model and the vertically homogeneous water column have been carefully discussed. This research suggests that $E_{0,PAR}(z)$ can be obtained routinely from ocean-color data and may have significant implications for the estimation of global heat and carbon budget.

2. Methods

2.1 *Fast, accurate model of underwater scalar irradiance*

Liu *et al.* (2002) employed four strategies to accelerate the simulation of the underwater light field without losing accuracy compared with the latest version 4.2 of

Hydrolight (H42). They demonstrated that the sky radiance can be reallocated to the plane of the Sun and decomposed into ten independent sources of light incident from ten different zenith angles. $E_{0,PAR}(z)$ can then be obtained by summation of contributions from these light sources. For each incident light source with unit intensity, they constructed a look-up table (LUT) for quick reference to a set of parameters (B_0, B_1, P, B_2, Q) that are required by a five-parameter model (McCormick, 1995) for specifying the vertical profile of the average cosine $\bar{\mu}(z)$. Finally, Gershun's equation (Gershun, 1939) was used to convert $\bar{\mu}(z)$ to $E_0(z)$. They also developed an empirical approach to correct the effects of a wind-roughened surface and the contributions from an extra CDOM component. Their model runs more than fourteen thousand times faster than the full Hydrolight code, while limiting the percentage error to 2.20% and the maximum error to less than 4.78%. Detailed procedures are illustrated in the block of Step 3 of Fig. 2.

To construct a LUT of $\bar{\mu}(z)$, Liu *et al.* (2002) employed a set of bio-optical models to parameterize IOPs, including absorption, scattering, and the phase scattering function. The absorption coefficient $a(\lambda)$ is obtained using the models of Morel (1991) and Prieur and Sathyendranath (1981):

$$a(\lambda) = a_w(\lambda) + 0.06 a_c^*(\lambda) Chl^{0.65} + F \cdot 0.06 \cdot a_c^*(440) Chl^{0.65} \exp\left(-0.014(\lambda - 440)\right), \quad (2)$$

where $a_w(\lambda)$ is the absorption coefficient of pure water, Chl is the chlorophyll-a concentration (mg m^{-3}), F specifies how CDOM absorption is set to be proportional to chlorophyll absorption at a reference wavelength 440 nm, and $a_c^*(\lambda)$ is the normalized chlorophyll-specific absorption coefficient. $a_w(\lambda)$ is taken from Pope and Fry (1997). $a_c^*(\lambda)$ is given by Morel (1988) and is equal to unity at a reference wavelength 440 nm (i.e. $a_c^*(440) = 1$). Although F is usually set at a fixed value of 0.2 for Case 1 waters (Prieur and Sathyendranath, 1981; Morel, 1991), it may vary within a range around 0.2 (Liu *et al.*, 1999). We determine F from an estimate of the CDOM absorption coefficient at 440 nm $a_g(440)$. The scattering coefficient $b(\lambda)$ is derived from the model of (Gordon and Morel, 1983):

$$b(\lambda) = b_w(\lambda) + 0.30\left(\frac{550}{\lambda}\right) Chl^{0.62}, \quad (3)$$

where $b_w(\lambda)$ is the spectral scattering coefficient of pure water as taken from (Morel, 1974). The normalized phase scattering function $\tilde{\beta}$ is the sum of the contributions by pure water and particles (Mobley, 1994)

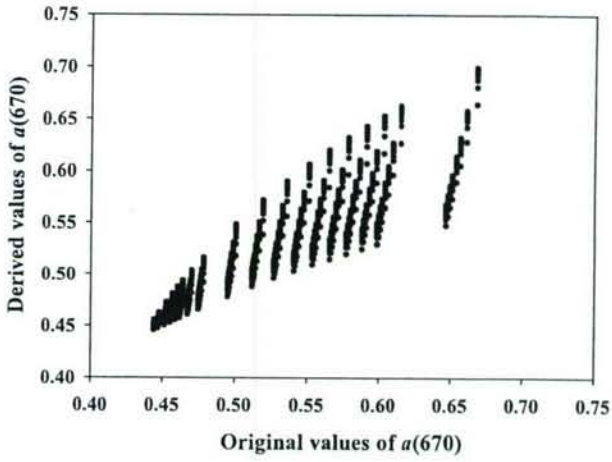

Fig. 1. Comparison of derived $a(670)$ (Eq. (1)) and original values of the simulated data.

$$\tilde{\beta}(\psi;\lambda) \equiv \frac{b_w(\lambda)}{b(\lambda)} \tilde{\beta}_w(\psi) + \frac{b_p(\lambda)}{b(\lambda)} \tilde{\beta}_p(\psi;\lambda), \quad (4)$$

where ψ is the scattering angle and $b_p(\lambda)$ is the spectral scattering coefficient of particles. $\tilde{\beta}_w(\psi)$ and $\tilde{\beta}_p(\psi;\lambda)$ are calculated from the analytic Fournier-Forand phase function (Fournier and Forand, 1994) by specifying the backscatter fraction of water BF_w and particles BF_p, respectively. The value of BF_w is set to be 0.5 (Mobley and Sundman, 2001).

This set of three-variable (Chl, F, BF_p) bio-optical models gives a flexible parameterization of IOPs representative of a large variety of water types. The current LUT is constructed by changing variables within certain ranges: λ (400–700 nm), Chl (0–10 mg m^{-3}) and BF_p (0.01–0.04) (Liu *et al.*, 2002). Note that there is no limitation on the range of F by employing an empirical approach to correct the contributions from an extra CDOM component.

In principle, the model of Liu *et al.* (2002) can be integrated with any ocean color algorithms. We present here the integration of their model and the quasi-analytical algorithm (QAA) (Lee *et al.*, 2002), with the goal of improving the retrievals of Chl, F and BF_p, and hence, the estimation of $E_{0,PAR}(z)$ from the spectrum of remote sensing reflectance measured above the surface $R_{rs}(\lambda)$.

2.2 *Quasi-analytical algorithm*

A full description of the QAA is presented by Lee *et al.* (2002). Briefly, the QAA employs a series of analytical, semi-analytical and empirical algorithms to convert $R_{rs}(\lambda)$ to $a(\lambda)$ and $b_b(\lambda)$. Multiple H42 simulations were done to derive the empirical relationship between $a(670)$

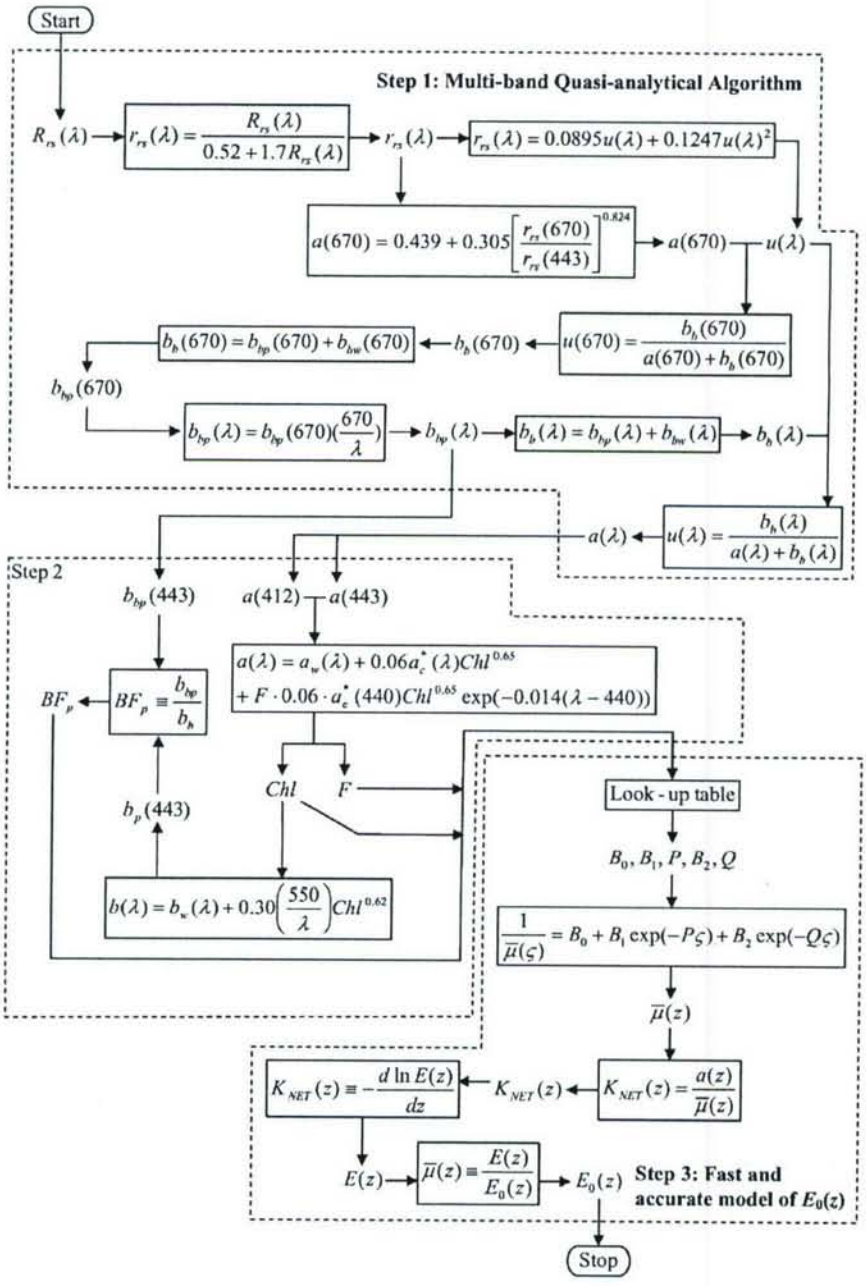

Fig. 2. Processing steps to convert $R_{rs}(\lambda)$ to $E_0(z)$.

and the ratio of $r_{rs}(670)$ and $r_{rs}(443)$ by varying the three variables within the ranges Chl (0–10 mg·m^{-3}), F (0–1.0) and BF_p (0.005–0.05), where r_{rs} stands for the remote sensing reflectance measured just below the surface. A regression analysis gives

$$a(670) = 0.439 + 0.305\left[\frac{r_{rs}(670)}{r_{rs}(443)}\right]^{0.824}. \quad (5)$$

The comparison of the derived $a(670)$ and their original values of simulated data is shown in Fig. 1. Even at band 670 nm, where absorption is mainly dominated by water, varying the volume scattering phase function (VSF) through BF_p has an effect on r_{rs}, and hence the derived $a(670)$. The simple regression analysis shown here (Eq. (5)) provides a good estimation of $a(670)$. Recent work by Lee and Sandidge (2003) employed a neural network approach to relate a to the spectral ratio of r_{rs}. Therefore,

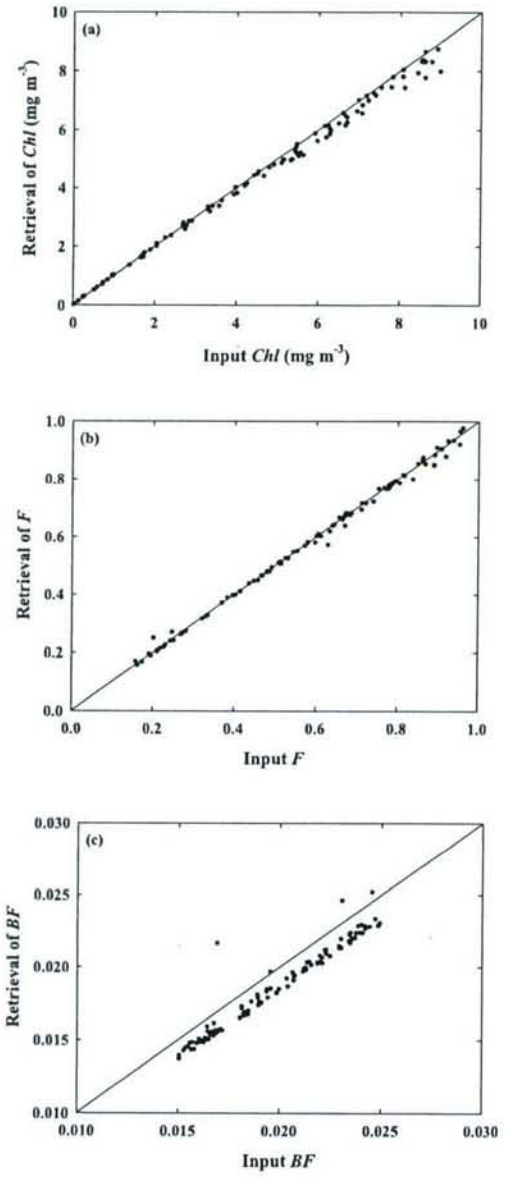

Fig. 3. Comparison between retrieval of (a) *Chl*, (b) F and (c) BF_p using QAA and original values used in H42 simulations. A total of 100 cases were compared by randomly specifying values of the solar zenith angle (0°–45°), percent cloud cover (0–50%), surface wind speed (0–15 m/s), chlorophyll concentration (0–9 mg m^{-3}), visibility (5–50 km), the CDOM ratio F (0.15–1.0) and backscatter fraction BF_p (0.015–0.025).

the deviations shown in Fig. 1 can be reduced.

QAA was derived from a large combination of IOPs for a wide variety of water types. It should be applicable to Case 1 waters of which the IOPs are described by a set of three-variable biooptical models (Eqs. (2)–(4)). The accuracy of QAA in retrieving (*Chl*, F, BF_p) was first examined by use of Hydrolight-simulated $R_{rs}(\lambda)$ curves. Detailed procedures are illustrated in the block of Step 1 of Fig. 2.

Table 2. Accuracy of retrievals for simulations shown in Fig. 3.

Index	*Chl*	F	BF_p
Pearson correlation coefficient	0.998	0.998	0.967
Average value of relative error (%)	5.19	1.73	6.78

A total of 100 cases were simulated by randomly specifying values of seven parameters (see caption of Fig. 3 for details). For each case, H42 was run to simulate R_{rs} at 20 wavebands in the PAR range (default setting in H42 for simulating SeaWiFS). Note that all processes of inelastic scattering are considered and the fluorescence efficiencies are the default settings in H42. The simulated $R_{rs}(\lambda)$ were then used as input to QAA for converting $R_{rs}(\lambda)$ to $a(\lambda)$ and $b_b(\lambda)$. The algebraic solutions of *Chl*, F and BF_p can be obtained from $a(412)$, $a(443)$ and $b_b(443)$ (see the block of Step 2 of Fig. 2). The retrievals of *Chl*, F and BF_p and their original values are compared in Fig. 3, and the average values of the relative error for retrieving *Chl*, F and BF_p are listed in Table 2.

2.3 Field data

In situ data were collected during EcoHAB cruises between March 1999 and October 2001 on the West Florida Shelf, and the Coastal Benthic Optical Properties (CoBOP) experiment from 1998 to 2000 in late May to early June around Lee Stocking Island in the Bahamas. $R_{rs}(\lambda)$ was determined by correcting for the surface-reflected skylight and solar glint from the above-surface total reflectance, which is measured from a hyper-spectral handheld radiometer (Spectrix) developed by the University of South Florida. The details of the method are given in Lee *et al.* (1998). The vertical profile of $E_d(z)$ was measured using a submersible hyperspectral radiometer that was also developed by the University of South Florida. This instrument, together with two ac-9™ absorption meters (WET Labs) and a Hydroscat-6™ backscattering meter (HOBI Labs) were deployed on a slow-drop package and allowed to drift away from the boat to minimize ship shadow.

Surface water samples were collected at each station. The spectrophotometric methods consisted of summing the particulate absorption (a_p) as determined by the quantitative filter pad method (Bissett *et al.*, 1997) and the absorption of the 0.22 μm filtrate (a_g) as measured using a 10 cm cell in a Perkin Elmer Lambda 18 spectrophotometer (Spec). The accuracy of the a_g measurement

Table 3. Descriptions of the *in situ* data used in the model-to-data comparison (Figs. 4 and 5).

Originator identifier	LSD52601	LK404U	Mirir1	Mirir2
Location	LSI (23.81°N, 76.06°W)	WFS (26.98°N, 83.30°W)	(28.79°N, 89.84°W)	(28.68°N, 89.90°W)
Water type	Low Chl-*a* Moderate CDOM	Moderate Chl-*a* Moderate CDOM	High Chl-*a* High CDOM	Moderate Chl-*a* High CDOM
Date	26-May-00	22-Apr-01	7-Apr-00	26-Oct-00
Time (GMT)	13:57	18:03	14:10	16:37
Solar zenith angle (degree)	34.9	27.48	58.6	44.2
Cloudiness (%)	10.0	5.0	30.0	5.0
Mean wind speed (m/s)	6.00	7.96	10.0	5.0
Average BP ("Hg)	29.92*	30.26	29.92*	29.92*
Air mass type	1*	1*	1*	1*
Average relative humidity (%)	80*	79.7	80*	80*
Precipitable water content (cm)	1.5*	1.5*	1.5*	1.5*
Visibility (km)	15.0*	15.0*	15.0*	15.0*

*Default values used in Hydrolight.

is $\pm 0.046\ m^{-1}$ as reported by the manufacturer's specifications. Chlorophyll concentrations were determined from the same samples using a Turner fluorometer (Holm-Hansen and Riemann, 1978). Details of the instruments and data processing of these two stations are described in Ivey *et al.* (2002).

To validate our approach, we need a set of field data with biological measurement of Chl-$a(z)$, the above-water measurement of $R_{rs}(\lambda)$, and the in-water measurement of IOPs(z). Apart from the profiles of $a(z, \lambda)$ and $c(z, \lambda)$ from the ac-9™ absorption meter (WET Labs), we especially need the backscattering coefficient $b_b(z, \lambda)$ for calculating the backscatter fraction $BF(z, \lambda)$. At the time of writing, there are only two stations (LSD52601 and LK404U) with b_b profiles measured from the newly installed Hydroscat-6™ backscattering meter (HOBI Labs). Therefore, we add the data from other two stations (Mirir1 and Mirir2) that have all measurements except for $b_b(z, \lambda)$. These measurements were obtained during a cruise in the northern Gulf of Mexico in 2001. Details of the instruments and data processing of these two stations are described in D'Sa and Miller (2003).

All field data were obtained from coastal regions, where LSD52601 and LK404U represent more clear waters with moderate chlorophyll and sediment loading, while Mirir1 and Mirir2 represent more turbid waters with high chlorophyll and sediment loading. A detailed description of all stations, including their locations and water types, is given in Table 3. Note that the model of Liu *et al.* (2002) can be applied to Case 1 waters as well as to Case 2 waters that is gelbstoff rich, and the volume-scattering phase function can be generated dynamically based on the backscatter fraction. Therefore, all field data collected in these four stations are valid inputs for the model of Liu *et al.* (2002) to estimate the underwater light field.

3. Results and Discussion

3.1 Model-to-data comparison

Here we present the results of model-to-data comparison at all stations. Following the Steps 1 and 2 illustrated in Fig. 2, the spectrum information of $R_{rs}(\lambda)$ is substituted into QAA to retrieve *Chl*, *F*, and BF_p. Since $R_{rs}(\lambda)$ is a weighted average signal over depths, the mean (hollow symbols) as well as the standard deviation (error bars) of the *in situ* measurements are calculated over the e-folding depth and compared to the retrievals of QAA (filled symbols), respectively (Fig. 4). The e-folding depth is defined as the depth where $E_{0,PAR}(z)$ has decreased to 1/e of its surface value. Note that we compare BF_p at band 488 nm because it is the first waveband that both ac-9 and Hydroscat-6 have. We also compare the total absorption coefficient at 440 nm, which takes into account the CDOM absorption through the value of F (Eq. (2)). For the case of the most turbid water at station Mirir1 (Fig. 4(c)), the deviations between the QAA retrievals and the means of *in situ* measurements taken within the e-folding depth (only 1.8 m) are apparent. The deviation can be reduced if the means are taken over more depths. However, there is no way to determine to what depths the means should be taken simply based on the existing measurements, because $R_{rs}(\lambda)$ is a weighted average signal over depths. Nevertheless, Fig. 4 demonstrates that QAA provides reasonable retrievals of bulk IOPs both for vertically well-mixed waters (Fig. 4(a)) and for those cases with vertical structure (Figs. 4(b), (c), (d)). These

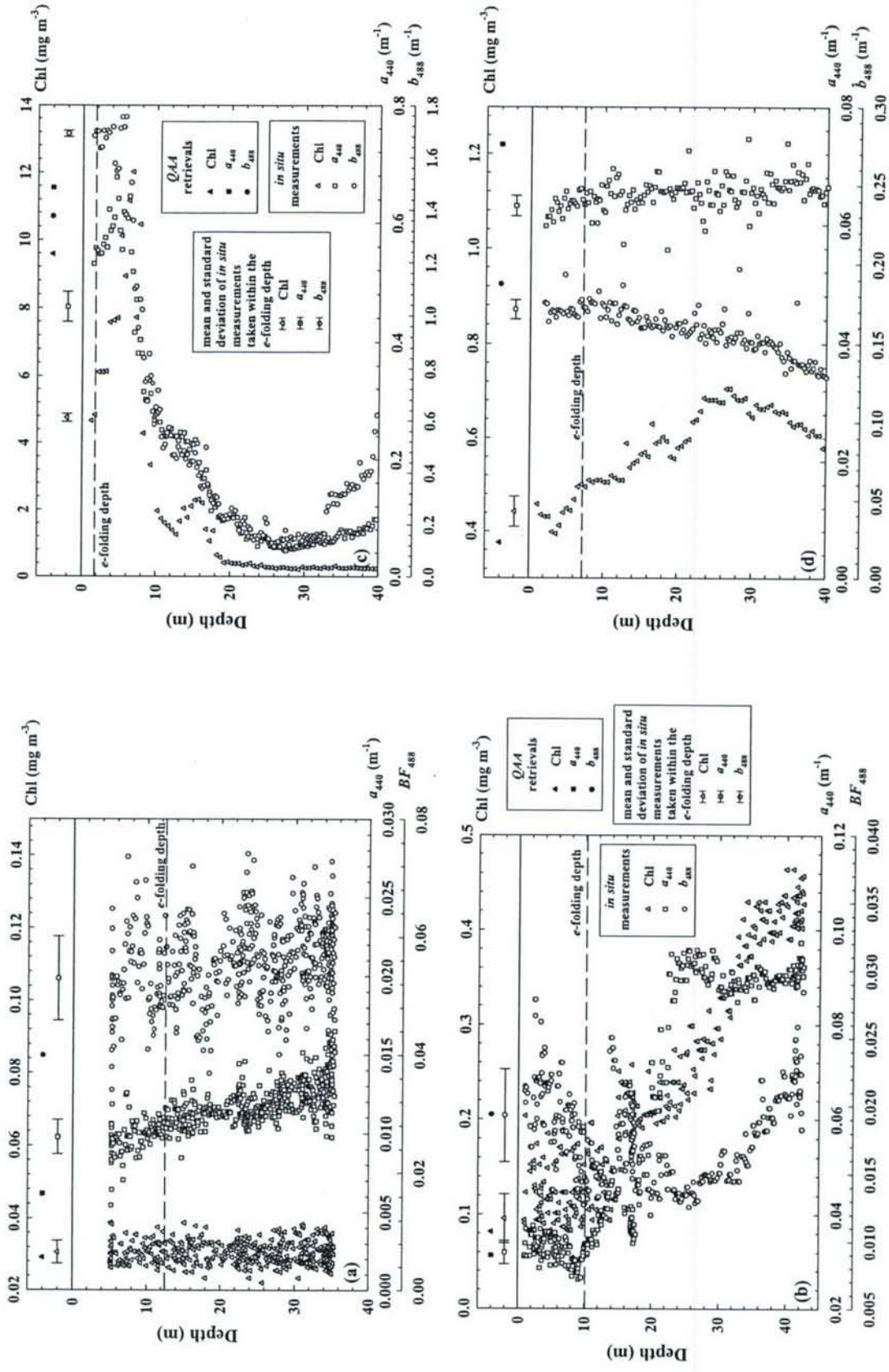

Fig. 4. Model-to-data comparison of IOPs. (a) LSD52601, (b) LK404U, (c) Mirir1 and (d) Mirir2.

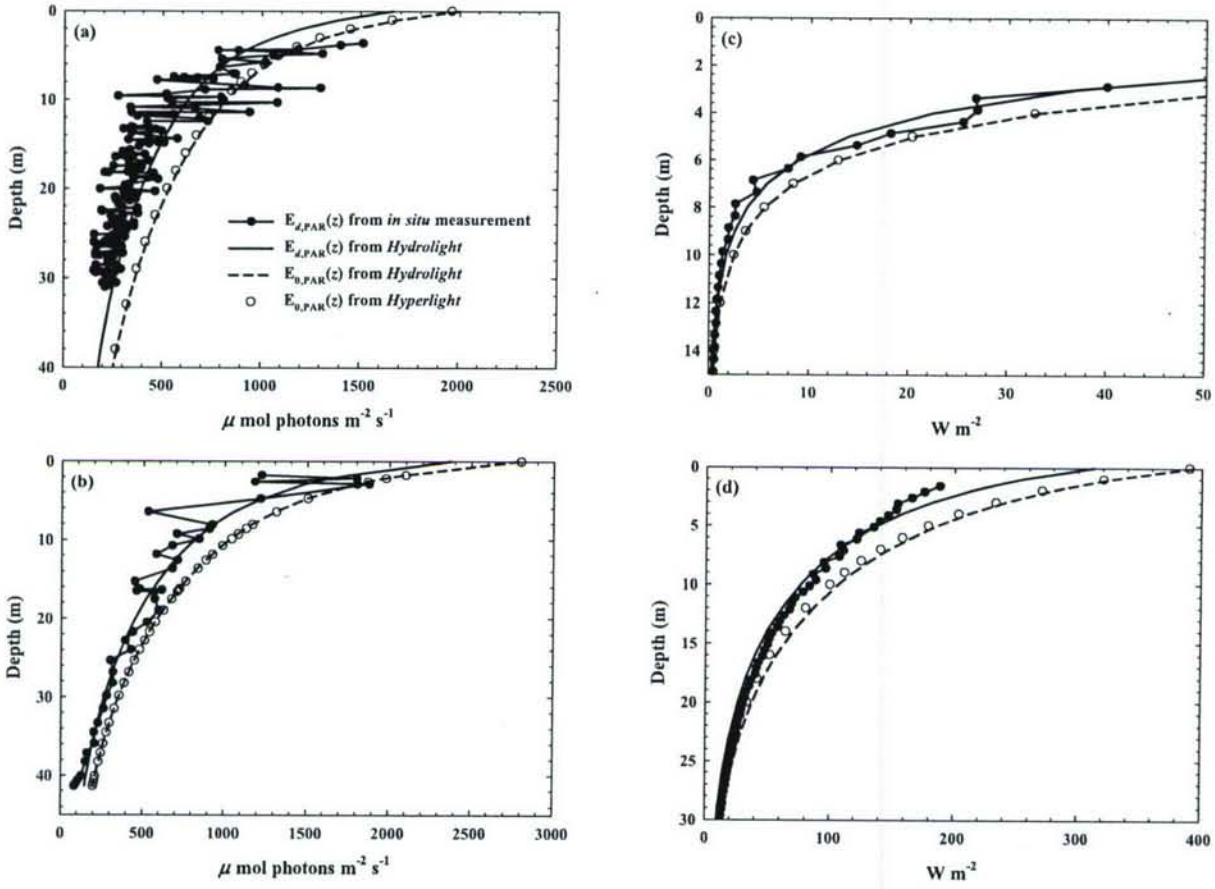

Fig. 5. Model-to-data comparison of the underwater light field. (a) LSD52601, (b) LK404U, (c) Mirir1 and (d) Mirir2.

retrievals are used as inputs to the model of Liu *et al.* (2002) to calculate $E_{0,PAR}(z)$, which corresponds to the *in situ* measurements well (Fig. 5).

As mentioned, light absorption by phytoplankton or other water constituents generally have no preferential direction (Kirk, 1994). Therefore, we should take the scalar irradiance E_0 rather than the downwelling planar irradiance E_d into account. Because the *in situ* measurements are $E_{d,PAR}(z)$ which cannot be compared directly to our model output $E_{0,PAR}(z)$, we use H42 as a surrogate to simulate both $E_{0,PAR}(z)$ and $E_{d,PAR}(z)$ under the same computational conditions. Figure 5 shows that, using the retrievals of *Chl*, F and BF_p from QAA, H42 offers a simulation of $E_{d,PAR}(z)$ that corresponds closely to the *in situ* measurements. In the meantime, the results from the model of Liu *et al.* (2002) are virtually identical to H42 simulations of $E_{0,PAR}(z)$. This comparison verifies our approach.

A major premise of this work is the vertical homogeneity of IOPs, which is not always valid (e.g. Figs. 4(b) and (c)). There is currently no practical way to resolve the vertical structure simply from surface observations of R_{rs}. The spectrum of R_{rs} should be signals weighted by $K_d(\lambda)$ over the first optical attenuation length, dependent on wavelength and the optical properties of the water at that wavelength (Platt and Sathyendranath, 1988). Nevertheless, both the OC2-v4 algorithm and our approach provide good retrievals that represent the bulk properties in the upper ocean. The model-to-data comparison demonstrates that a good estimate of $E_{0,PAR}(z)$ at depth can be obtained, as long as the bulk values of IOP are retrieved for the important surface layer. A detailed distribution of the IOPs in the vertical direction would be of great help in estimating $E_{0,PAR}(z)$ at depths. However, such information usually derives from simulations of biogeochemical models rather than remote sensing (e.g. see Bissett *et al.*, 1999). The model of Liu *et al.* (2002) needs to be further expanded to deal with a stratified water column, if the goal is to incorporate the optical model into a biogeochemical model.

Figure 5 also illustrates the difficulties in obtaining a smooth profile of $E_{d,PAR}(z)$ from *in situ* measurements. The irradiance fluctuation is a typical phenomenon that

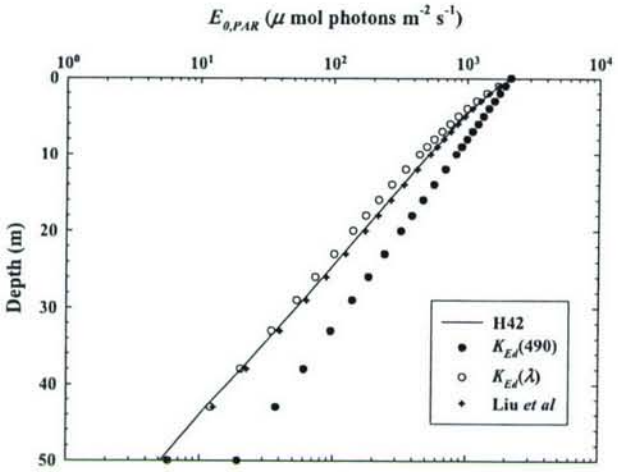

Fig. 6. Model-to-model comparison of $E^{X}_{0,PAR}(z)$, where X represents various approaches, including *H42* (Hydrolight version 4.2), $K_{Ed}(490)$ (Mueller, 2000), $K_{Ed}(\lambda)$ (Eq. (6)), and Liu *et al.* (this work).

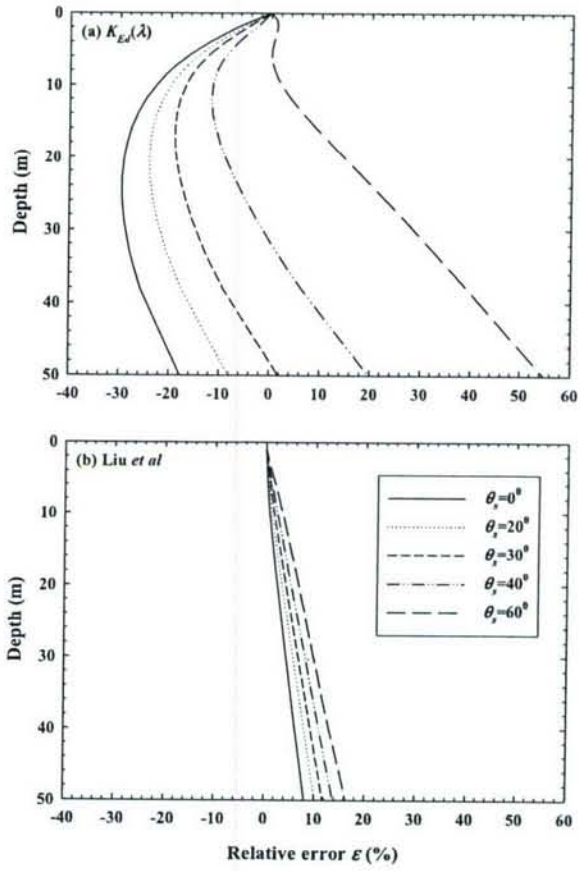

Fig. 7. Model-to-model comparison of the relative errors $\varepsilon(z)$ in predicting $E_{0,PAR}(z)$ by use of (a) $K_{Ed}(\lambda)$ approach, and (b) Liu *et al.* approach. The controlled variable θ_s is varied from 0° to 60°.

is not due to small-scale vertical variations in the IOPs but almost entirely due to the wavy surface (Zaneveld *et al.*, 2001). Another limitation of the model-to-data comparison is that the dataset collected from *in situ* measurements only covers a limited range of IOPs. To further verify our approach for a large variety of water types, we conducted the following model-to-model comparisons.

3.2 *Model-to-model comparison*

The procedure used for model-to-model comparisons is briefly as follows. For a set of computational conditions of IOPs and the ambient optical environment, the H42 radiative transfer model (Mobley and Sundman, 2001) is used to simulate $L_w(490)$, $L_w(555)$ and $R_{rs}(\lambda)$. A detailed vertical profile of $E^{\mathrm{H42}}_{0,PAR}(z)$ is also generated to represent the simulated underwater light field derived from a full solution of the radiative transfer equation. The latest formula (Mueller, 2000) is used to calculate $K_{Ed}(490)$ from $L_w(490)$ and $L_w(555)$. The ratio of E_0/E_d is nominally 1.4–1.8 up to 2.0–2.5 in very turbid waters (Kirk, 1994). Therefore, $K_{Ed}(490)$ is assumed to approximate $K_{0,PAR}$ averaged over the entire PAR spectral range and depth, and $E^{K_{Ed}(490)}_{0,PAR}(z)$ is estimated by attenuating the below-surface value of $E_{0,PAR}(0^-)$ by $K_{Ed}(490)$. Austin and Petzold (1986) found a relationship:

$$\frac{K_{Ed}(\lambda)-K_{Ed,water}(\lambda)}{K_{Ed}(490)-K_{Ed,water}(490)}=M(\lambda), \qquad (6)$$

which allows us to estimate $K_{Ed}(\lambda)$ from $K_{Ed}(490)$. Therefore, another profile $E^{K_{Ed}(\lambda)}_{0,PAR}(z)$ can be obtained by attenuating the below-surface value of $E_{0,PAR}(0^-)$ by $K_{Ed}(\lambda)$. Finally, the H42 simulated $R_{rs}(\lambda)$ and $E_d(\lambda, 0^+)$ curves are used to calculate $E^{\mathrm{Lcc\ et\ al}}_{0,PAR}(z)$ following the approach illustrated in Fig. 2.

We start from a simulation of a typical Case 1 water and compare the predictions of $E_{0,PAR}(z)$ using different approaches (Fig. 6). A detailed description of this set of computational conditions is given in the caption of Fig. 6. The relative errors of $E^{K_{Ed}(490)}_{0,PAR}(z)$ are as high as 188.0% at the euphotic depth (38.0 m), while $E^{\mathrm{Lcc\ et\ al}}_{0,PAR}(z)$ closely matches the full H42 solution $E^{\mathrm{H42}}_{0,PAR}(z)$ (8.1% at the same depth). $E^{K_{Ed}(\lambda)}_{0,PAR}(z)$ indeed gives a better prediction than $E^{K_{Ed}(490)}_{0,PAR}(z)$ by taking the spectral variation of $K_{Ed}(\lambda)$ into consideration. However, apparent deviations between $E^{K_{Ed}(\lambda)}_{0,PAR}(z)$ and $E^{\mathrm{H42}}_{0,PAR}(z)$ can still be seen from 5 m to 30

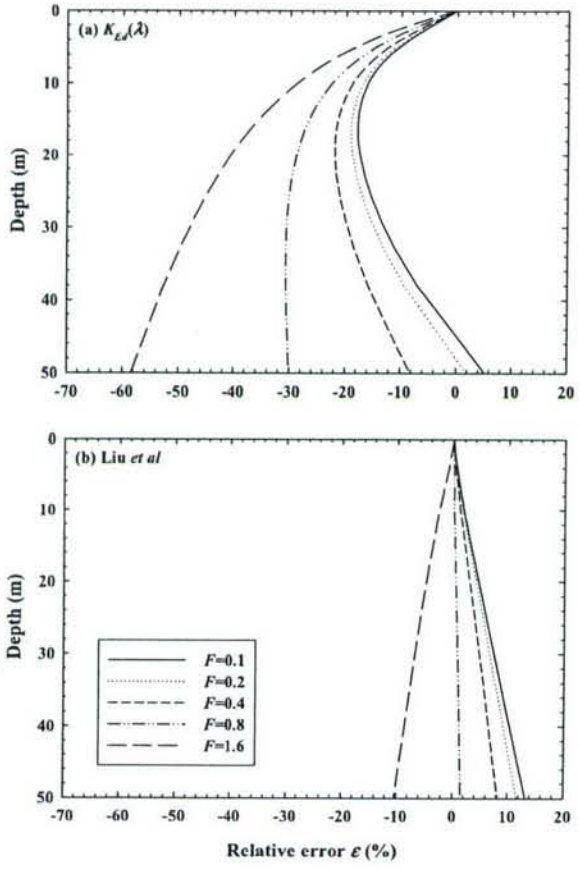

Fig. 8. As Fig. 7 except that the controlled variable F is varied from 0.1 to 1.6.

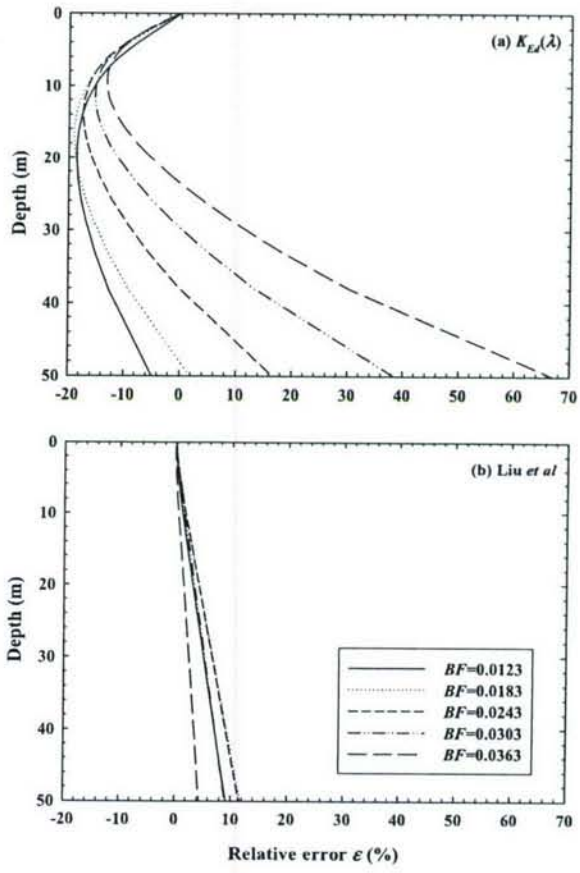

Fig. 9. As Fig. 7 except that the controlled variable BF is varied from 0.0123 to 0.0363.

m. The relative error of $E_{0,PAR}^{K_{Ed}(\lambda)}(z)$ reaches a maximum value of 17.0% at the depth of 14.0 m, while the relative error of $E_{0,PAR}^{\text{Lcc et al}}(z)$ is merely 2.1% at the same depth. This error, as mentioned above, resulted from neglecting the variation of K_{Ed} with depth. To validate our approach and assess the error that might result from other sources, we extend the model-to-model comparison by varying one computational condition at a time and keeping the others the same as those used in Fig. 6.

Figure 7 shows the result of varying the solar zenith angle θ_s from 0° to 60°, which can be used to illustrate the variation of the underwater light field within one day. Even for a typical Case 1 water, θ_s has a significant effect on $E_{0,PAR}(z)$ that cannot be modeled accurately using the $K_{Ed}(\lambda)$ approach. The relative errors range from –30.0% to 54.9% at different depths (Fig. 7(a)). By contrast, our approach gives an estimation that reduces the relative error (0 to 16.3%), regardless of the different θ_s used (Fig. 7(b)). Varying the solar zenith angle θ_s would have similar effects on the simulation of underwater light field to varying other parameters of incident light field, such as the surface wind speed, visibility, cloudiness, etc.

Figure 8 gives the result of changing the CDOM ratio F from 0.1 to 1.6. The relative errors range from –58.4% to 5.2% at different depths (Fig. 8(a)). By contrast, our approach gives an estimation that reduces the relative error (–10.3% to 13.9%), regardless of the different F used (Fig. 8(b)). Figure 9 shows the result of changing the backscatter fraction BF_p from 0.0123 to 0.0363. The relative errors range from –19.0% to 66.9% at different depths (Fig. 9(a)). By contrast, our approach gives an estimation that reduces the relative error (–0.8% to 11.4%), regardless of the different BF_p used (Fig. 9(b)). The $K_{Ed}(\lambda)$ approach (Eqs. (1) and (6)) is developed for Case 1 waters. If the IOPs are deviated from the assumption of Case 1 waters, it is expected that using the $K_{Ed}(\lambda)$ approach to predict $E_{0,PAR}(z)$ will generate a significant error (Figs. 8(a) and 9(a)). By contrast, our approach provides an estimation that closely matches the full H42 solution, regardless of the different values of F or BF_p used (Figs. 8(b) and 9(b)). Varying the CDOM ratio F or the

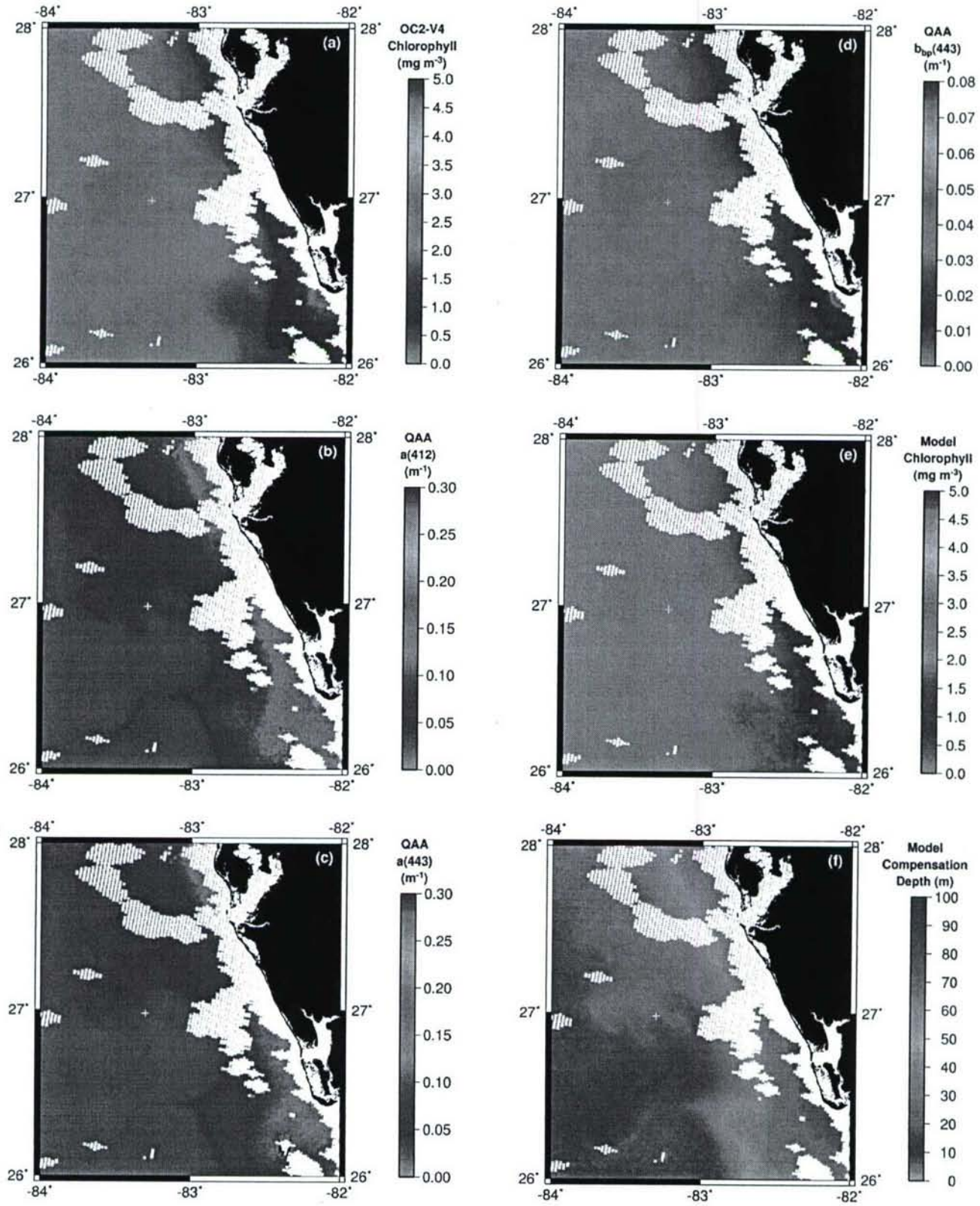

Fig. 10. Applications in processing SeaWiFS imagery taken during the EcoHAB cruises in 2001 on the West Florida Shelf. (a) Chlorophyll-*a* concentration (SeaWiFS OC2V4 algorithm), (b) Chlorophyll-*a* concentration (Liu *et al.*), (c) $a(443)$ (Liu *et al.*), (d) $b_{bp}(443)$ (Liu *et al.*), (e) Chlorophyll-*a* concentration (Liu *et al.*), and (f) D_c (Liu *et al.*).

backscatter fraction BF_p would have similar effects on the simulation of underwater light field to varying other parameters of water constituents, such as the chlorophyll concentration.

4. Processing SeaWiFS Imagery

The newly-developed approach was applied to process SeaWiFS imagery taken during the EcoHAB cruises in 2001 on the West Florida Shelf. Figure 10(a) shows the distribution of chlorophyll-*a* concentration derived from the standard SeaWiFS OC2V4 algorithm. The white areas indicate those pixels that are either masked by cloud or failed the quality test, while the white cross mark pinpoints the place where the *in situ* measurements (Figs. 4(b) and 5(b)) were made. Since our approach only requires $a412$, $a443$ and $b_{bp}443$ (see Step 2 in Fig. 2), the retrievals of these values by use of QAA are shown in Figs. 10(b), (c) and (d), respectively. As expected, the distribution illustrates the influences of coastal runoff on the IOPs. The retrieval of chlorophyll-*a* concentration following Step 2 of Fig. 2 is illustrated in Fig. 10(e). Compared to the results of OC2V4, our approach gives comparable values of *Chl* in general. Figure 10(f) shows the depth of the euphotic zone where $E_{0,PAR}$ equals 1% of the subsurface value of $E_{0,PAR}$. This depth is usually treated as an approximation of the compensation depth D_c (Mann and Lazier, 1996), which plays a significant role in the ecosystem of phytoplankton. Failure to correctly estimate the underwater light field, and hence the compensation depth, will generate significant errors in modeling the plankton ecosystem.

5. Conclusions

Regional to global estimates of the underwater light field are required to develop realistic models of ocean primary productivity, and heat and carbon fluxes. To date, most attempts to incorporate satellite ocean-color data are based on a simple, but error-prone $K_{Ed}(490)$ model. We present a new approach that incorporates two models (Lee *et al.*, 2002; Liu *et al.*, 2002) to estimate the underwater light field from remote sensing of ocean color. A thorough model-to-data and model-to-model comparison was performed to verify this new approach. We successfully mapped the compensation depth by applying this new approach to process SeaWiFS imagery. The current model of $E_{0,PAR}(z)$ is limited to a vertically homogeneous water column with variables in certain ranges: λ (400–700 nm), *Chl* (0–10 mg m^{-3}) and BF_p (0.01–0.04) (Liu *et al.*, 2002). Future work will improve the model by removing some of the limitations, and develop a better scheme of inversion to retrieve IOPs. This work indicates that incorporating two models (Lee *et al.*, 2002; Liu *et al.*, 2002) may provide large-scale estimates of the underwater light field that, while not perfect, are significantly more accurate than a K_{Ed} approach and computationally feasible for the generation of routine products. The product of $E_{0,PAR}(z)$ can be obtained routinely from ocean-color data and may have significant implications for the estimation of global heat and carbon budget.

Acknowledgements

Part of this work was performed while C.-C. Liu held a National Research Council Research Associateship at NASA John C. Stennis Space Center. This work was also supported by the National Science Council of Taiwan (NSC 94-2611-M-006-002). We thank Dr. I-I Lin for many useful comments. The computer facility and hand-held radiometer provided by National Center for Oceanography Research of Taiwan are appreciated.

Appendices

Symbol	Units	Description
a	m^{-1}	total absorption coefficient
$a_c^*(\lambda)$		normalized chlorophyll-specific absorption coefficient
a_g	m^{-1}	absorption coefficient of CDOM
a_w	m^{-1}	absorption coefficient of pure water
B_0		parameter required for McCormick model of $\overline{\mu}(z)$
B_1		parameter required for McCormick model of $\overline{\mu}(z)$
B_2		parameter required for McCormick model of $\overline{\mu}(z)$
BF		backscatter fraction
BF_p		backscatter fraction of particles
BF_w		backscatter fraction of water
b	m^{-1}	total scattering coefficient
b_b	m^{-1}	backscattering coefficient
b_p	m^{-1}	scattering coefficient of particles
b_w	m^{-1}	scattering coefficient of pure water
Chl	mg m^{-3}	chlorophyll-*a* concentration
D_c	m	compensation depth
E_0	Wm^{-2}sr^{-1}	scalar irradiance
$E_{0,PAR}$	Wm^{-2}sr^{-1}	wavelength-integrated scalar irradiance in the PAR range
E_d	Wm^{-2}sr^{-1}	downwelling planar irradiance
$E_{d,PAR}$	Wm^{-2}sr^{-1}	wavelength-integrated downwelling planar irradiance in the PAR range
F		CDOM ratio
L	Wm^{-2}sr^{-1}nm^{-1}	radiance
L_w	Wm^{-2}sr^{-1}nm^{-1}	water-leaving radiance
K_{Ed}	m^{-1}	total diffuse attenuation coefficient for downwelling planar irradiance
$K_{Ed,water}$	m^{-1}	same as K_{Ed} but for pure water
P		parameter required for McCormick model of $\overline{\mu}(z)$
Q		parameter required for McCormick model of $\overline{\mu}(z)$
R_{rs}		the remote sensing reflectance measured just above the surface
r_{rs}		the remote sensing reflectance measured just below the surface

$\tilde{\beta}$		normalized phase scattering function
$\tilde{\beta}_w$		normalized phase scattering function of pure water
$\tilde{\beta}_p$		normalized phase scattering function of particles
λ	nm	wavelength
μ		average cosine
θ_s	degree	solar zenith angle
ψ	radian	scattering angle

References

Austin, R. W. and T. J. Petzold (1981): The determination of the diffuse attenuation coefficient of sea water using the Costal Zone Color Scanner. p. 239–256. In *Oceanography from Space*, ed. by J. F. R. Gower, Plenum Press, New York.

Austin, R. W. and T. J. Petzold (1986): Spectral dependence of the diffuse attenuation coefficient of light in ocean waters. *Optical Engineering*, **25**, 471–479.

Bissett, W. P., J. S. Patch, K. L. Carder and Z. P. Lee (1997): Pigment packaging and Chl a specific absorption in high-light oceanic waters. *Limnol. Oceanogr.*, **42**, 961–968.

Bissett, W. P., K. L. Carder, J. J. Walsh and D. A. Dieterle (1999): Carbon cycling in the upper waters of the Sargasso Sea: II. Numerical simulation of apparent and inherent optical properties. *Deep-Sea Res. I*, **46**, 271–317.

Carder, K. L., F. R. Chen, Z. P. Lee, S. K. Hawes and D. Kamykowski (1999): Semianalytic moderate-resolution imaging spectrometer algorithms for chlorophyll a and absorption with bio-optical domains based on nitrate-depletion temperatures. *J. Geophys. Res.*, **104**, 5403–5421.

D'Sa, E. J. and R. L. Miller (2003): Bio-optical properties in waters influenced by the Mississippi River during low flow conditions. *Remote Sensing of Environment*, **84**, 538–549.

Fournier, G. R. and J. L. Forand (1994): Analytic phase function for ocean water. *SPIE: Ocean Optics XII*, 194–201.

Gershun, A. (1939): The light field. *J. Math. Phys.*, **18**, 51–151.

Gordon, H. R. and A. Y. Morel (1983): *Remote Assessment of Ocean Color for Interpretation of Satellite Visible Imagery: A Review*. Springer-Verlag. New York.

Gordon, H. R., O. B. Brown, R. H. Evans, J. W. Brown, R. C. Smith, K. S. Baker and D. K. Clark (1988): A semianalytic radiance model of ocean color. *J. Geophys. Res.*, **93**, 10909–10924.

Holm-Hansen, O. and B. Riemann (1978): Chlorophyll-a determinations: improvement in methodology. *Oikos*, **30**, 438–447.

Hooker, S. B., W. E. Esaias, G. C. Feldman, W. W. Gregg and C. R. McClain (1992): An Overview of SeaWiFS and Ocean Color. p. 24. In *SeaWiFS Project Technical Report Series*, ed. by S. B. Hooker and E. R. Firestone, NASA Goddard Space Flight Center, Greenbelt, Maryland, U.S.A.

Ivey, J. E., K. L. Carder, F.-I. R. Chen and Z. Lee (2002): Absorption measurements in opticlly clear waters. *Ocean Optics XVI*.

Kirk, J. T. O. (1994): *Light and Photosynthesis in Aquatic Ecosystems*. Cambridge University Press, Cambridge, 509 pp.

Lee, Z. P. and J. Sandidge (2003): Ocean-color inversion: a combined approach by analytical solution and neural net. *Ocean Remote Sensing and Imaging*, SPIE5155, p. 153–161.

Lee, Z. P., K. L. Carder, R. G. Steward, T. G. Peacock, C. O. Davis and J. S. Patch (1998): An empirical algorithm for light absorption by ocean water based on color. *J. Geophys. Res.*, **103**, 27967–27978.

Lee, Z. P., K. L. Carder and R. A. Arnone (2002): Deriving inherent optical properties from water color: A multi-band quasi-analytical algorithm for optically deep waters. *Applied Optics*, **41**, 5755–5772.

Liu, C.-C., J. D. Woods and C. D. Mobley (1999): Optical model for use in oceanic ecosystem models. *Applied Optics*, **38**, 4475–4485.

Liu, C.-C., K. L. Carder, R. L. Miller and J. E. Ivey (2002): Fast and accurate model of underwater scalar irradiance. *Applied Optics*, **41**, 4962–4974.

Longhurst, A. (1995): An estimate of global primary production in the ocean from satellite radiometer data. *J. Plankton Res.*, **17**, 1245–1271.

Mann, K. H. and J. R. N. Lazier (1996): *Dynamics of Marine Ecosystems*. Blackwell, Oxford, 466 pp.

McCormick, N. J. (1995): Mathematical models for the mean cosine of irradiance and the diffuse attenuation coefficient. *Limnol. Oceanogr.*, **40**, 1013–1018.

Mobley, C. D. (1994): *Light and Water: Radiative Transfer in Natural Waters*. Academic Press, San Diego, CA, 592 pp.

Mobley, C. D. and L. K. Sundman (2001): Hydrolight 4.2 Users' Guide. Sequois Scientific, Inc., Redmond, WA, 87 pp.

Mobley, C. D., B. Gentili, H. R. Gordon, Z. Jin, G. W. Kattawar, A. Morel, P. Reinersman, K. Stamnes and R. H. Stavn (1993): Comparison of numerical models for computing underwater light fields. *Applied Optics*, **32**, 7484–7504.

Morel, A. (1974): Optical properties of pure water and pure sea water. p. 1–24. In *Optical Aspects of Oceanography*, ed. by N. G. Jerlov and E. S. Nielsen, Academic, New York.

Morel, A. (1988): Optical modelling of the upper ocean in relation to its biogenous matter content (case 1 water). *J. Geophys. Res.*, **93**, 10749–10768.

Morel, A. (1991): Light and marine photosynthesis: a spectral model with geochemical and climatological implications. *Prog. Oceanogr.*, **26**, 263–306.

Mueller, J. L. (1995): SeaWiFS Pre-launch algorithm for the diffuse attenuation coefficient K(490). San Diego State University Center for Hydro-Optics and Remote Sensing, San Diego, California, 11 pp.

Mueller, J. L. (2000): SeaWiFS algorithm for the diffuse attenuation coefficient, K(490), using water-leaving radiances at 490 and 555 nm. p. 24–27. In *SeaWiFS Project Postlaunch Technical Report Series*, ed. by S. B. Hooker and E. R. Firestone, NASA Goddard Space Flight Center, Greenbelt, Maryland, U.S.A.

Mueller, J. L. and C. C. Trees (1997): Revised SeaWiFS prelanuch algorithm for the diffuse attenuation coefficient K(490). p. 18–21. In *SeaWiFS Project Technical Report Series*, ed. by S. B. Hooker and E. R. Firestone, NASA Goddard Space Flight Center, Greenbelt, Maryland, U.S.A.

O'Reilly, J. E., S. Maritorena, B. G. Mitchell, D. A. Siegel, K. L. Carder, S. A. Garver, M. Kahru and C. Mcclain (1998):

Ocean color chlorophyll algorithms for SeaWiFS. *J. Geophys. Res.*, **103**, 24937–24953.

Platt, T. and S. Sathyendranath (1988): Oceanic primary production: estimation by remote sensing at local and regional scales. *Science*, **241**, 1613–1620.

Platt, T., S. Sathyendranath and A. Longhurst (1995): Remote sensing of primary production in the ocean: promise and fulfillment. *Philosophical Transactions of the Royal Society B*, **348**, 191–202.

Pope, R. M. and E. S. Fry (1997): Absorption spectrum (380–700 nm) of pure water. II. Integrating cavity measurements. *Applied Optics*, **36**, 8710–8723.

Prieur, L. and S. Sathyendranath (1981): An optical classification of coastal and oceanic waters based on the specific spectral absorption curves of phytoplankton pigments, dissolved organic matter, and other particulate materials. *Limnol. Oceanogr.*, **26**, 671–689.

Simpson, J. J. and T. D. Dickey (1981): Alternative parameterizations of downward irradiance and their dynamical significance. *J. Phys. Oceanogr.*, **11**, 876–882.

Zaneveld, J. R. V. (1989): An asymptotic closure theory for irradiance in the sea and its inversion to obtain the inherent optical properties. *Limnol. Oceanogr.*, **34**, 1442–1452.

Zaneveld, J. R. V., E. Boss and A. Barnard (2001): Influence of surface waves on measured and modeled irradiance profiles. *Applied Optics*, **40**, 1442–1449.